Title

Ultrasensitive amyloid β-protein quantification with high dynamic range using a hybrid graphene-gold surface-enhanced Raman spectroscopy platform.

Journal

Journal of Raman spectroscopy : JRS, 51(3)

ISSN

0377-0486

Authors

Yu, Xinke
Hayden, Eric Y
Wang, Pu
et al.

Publication Date

2020-03-01

DOI

10.1002/jrs.5785

Peer reviewed

Received: 16 May 2019 | Revised: 24 August 2019 | Accepted: 13 October 2019

DOI: 10.1002/jrs.5785

RESEARCH ARTICLE

Journal of RAMAN SPECTROSCOPY WILEY

Ultrasensitive amyloid β-protein quantification with high dynamic range using a hybrid graphene–gold surface-enhanced Raman spectroscopy platform

Xinke Yu[1] | Eric Y. Hayden[2] | Pu Wang[1] | Ming Xia[1] | Owen Liang[1] | Yu Bai[3] | David B. Teplow[2] | Ya-Hong Xie[1,4]

[1]Department of Materials Science and Engineering, University of California, Los Angeles, Los Angeles, California

[2]Department of Neurology, David Geffen School of Medicine, University of California, Los Angeles, Los Angeles, California

[3]School of Nano-Science and Nano-Engineering, Suzhou & Collaborative Innovation Center of Suzhou Nano Science and Technology, Xi'an Jiaotong University, Xi'an, China

[4]Jonsson Comprehensive Cancer Center, University of California, Los Angeles, Los Angeles, California

Correspondence
David Teplow, Department of Neurology, David Geffen School of Medicine, University of California, Los Angeles, Los Angeles, CA 90095.
Email: dteplow@mednet.ucla.edu

Ya-Hong Xie, Department of Materials Science and Engineering, University of California, Los Angeles, Los Angeles, CA 90095.
Email: yhx@ucla.edu

Funding information
Alexander von Humboldt-Stiftung Foundation; United States Government; Zhejiang University Cao Guangbiao High-Tech Talent Fund; National Institutes of Health, Grant/Award Numbers: AG041295, NS038328; Alexander von Humboldt Foundation, Grant/Award Number: NS038328

Abstract

Surface enhanced Raman spectroscopy (SERS) holds great promise in biosensing because of its single-molecule, label-free sensitivity. We describe here the use of a graphene–gold hybrid plasmonic platform that enables quantitative SERS measurement. Quantification is enabled by normalizing analyte peak intensities to that of the graphene G peak. We show that two complementary quantification modes are intrinsic features of the platform and that through their combined use, the platform enables accurate determination of analyte concentration over a concentration range spanning seven orders of magnitude. We demonstrate, using a biologically relevant test analyte, the amyloid β-protein (Aβ), a seminal pathologic agent of Alzheimer's disease, that linear relationships exist between (a) peak intensity and concentration at a single plasmonic hot spot smaller than 100 nm and (b) frequency of hot spots with observable protein signals, that is, the colocation of an Aβ protein and a hot spot. We demonstrate the detection of Aβ at a concentration as low as 10^{-18} M after a single 20 μl aliquot of the analyte onto the hybrid platform. This detection sensitivity can be improved further through multiple applications of analyte to the platform and by rastering the laser beam with smaller step sizes.

KEYWORDS

SERS, Amyloid, Graphene, Quantitation

Xinke Yu and Eric Y. Hayden are co-first authors.

1 | INTRODUCTION

The development of sensitive techniques for the detection and quantitative analysis of biomolecules[1–4] is important for trace element detection, environmental monitoring, and early stage diagnosis and treatment of diseases. Detection methods include high-performance liquid chromatography,[5] liquid chromatography mass spectrometry,[6] and enzyme-linked immunosorbent assays.[7] A limit of detection of 1 ng/ml has been achieved with these platforms, a sensitivity that is among the best currently achievable in biological sensing. Surface-enhanced Raman scattering (SERS) is a method that has gained increasing notice because of its ability to achieve single molecule detection with high molecular specificity[8–11] without the use of biological labels. Recent advances in nanotechnology have led to many SERS-based analytical applications. For example, self-assembled monolayer-coated colloidal gold platforms are able to detect Rhodamine 6G in the concentration range of 0.1–5 μM.[7] Metallic glassy nanowire arrays have a dynamic range of 1–10 nM for Rhodamine B.[12] Gold nanoparticles allow detection of glucose in the concentration range of 0.5–32 mM.[13]

Accurate analyte quantification using SERS has been challenging due primarily to the lack of a built-in marker of local electromagnetic (EM) field intensity, which is known to vary substantially from location to location on plasmonic surfaces currently in use.[14] Signal intensity depends on the local EM field intensity as well as analyte concentration.[15] This means that signal intensities measured at different points on a surface vary even if analyte concentration is constant. SERS signal intensity per se does not have a one-to-one correlation with analyte concentration. Such correlation could be established only if the EM field intensity at an individual plasmonic hot spot could be determined independent of analyte concentration. Prior studies have employed the assembly of marker molecules as internal standards.[13] However, the nonplanar topology typical of plasmonic surfaces, which can create local inhomogeneities in marker concentration significantly confounds the situation. In addition, the relatively large size of typical SERS internal standards (~50 nm)[7,16] relative to hot spot size can interfere with adsorption of the actual analyte at the hot spot, precluding Raman signal production by the analyte.

We report here the quantification ability of an ultrasensitive graphene-plasmonic hybrid platform[17] that largely eliminates these sources of variability. The platform incorporates a single atomic layer of graphene overlaying a gold surface consisting an array of nanopyramids, each of which is ~200 nm in width and height. Graphene deforms itself to conform to the substrate geometry via van der Waals forces.[17] The periodicity and size of individual pyramids are chosen for the optimization of surface plasmon resonance by laser excitation at 785 nm. The novelty of this work is that the single-layer graphene serves as an internal standard, which allows for accurate quantitation[9] and also provides additional Raman signal enhancement. Wang et al. demonstrated that the addition of a graphene monolayer on top of gold nanopyramids led to an enhancement of the Raman signal for small molecules (RG6) and proteins (lysozyme) and that by locating the areas of highest graphene peak intensity, they could more easily locate local hot spots, where the analyte signal also had the greatest enhancement.[17] SERS enhancement results primarily through an EM mechanism (up to 10^8 fold or 10^{14} fold in combination with resonance effects). A chemical mechanism also contributes to the enhancement due to the charge transfer between the analyte and graphene[18,19] and π–π stacking of aromatic molecules with π-bonds of graphene,[20] but to a much lesser degree (~10- to100-fold).[17]

We use the amyloid β-protein (Aβ), a well-studied pathologic agent of Alzheimer's disease,[21–23] as an example biologically relevant analyte to assess the potential of the hybrid platform for quantification and subsequent study of Aβ assembly dynamics. We observe two complementary quantification modes. The first (high analyte concentration regime) relates analyte concentration to the SERS peak intensity at individual SERS hot spots. The second (low concentration regime) relates analyte concentration to the probability of observing any Raman signal at any hot spot. In combination, these two modes enable analyte detection in a concentration range spanning seven orders of magnitude (10^{-18} to 10^{-15} M, 10^{-13} to 10^{-11} M).

2 | MATERIALS AND METHODS

2.1 | Chemicals and reagents

Unless specified otherwise, all chemicals and reagents were obtained from Sigma-Aldrich (St. Louis, MO) and were of the highest purity available.

2.2 | Substrate fabrication

The graphene–gold hybrid platform fabrication is based on sphere lithography, as previously reported.[24] The periodic gold nanopyramid structure with tunable size and sharpness is fabricated by a wafer-scale bottom-up templating technology. Spin-coated on (001) silicon

wafers, close-packed monolayer polystyrene balls with a diameter of 200 nm serve as templates. The pyramids form a quasiperiodic array of hexagonal arrangement that is uniformly distributed across the entire sample surface of 1 × 1-cm area. Because of the way the pattern is generated (self-assembly of polystyrene balls), variations in the spacing between pyramids, and the sizes of the pyramids themselves, can vary. This variance has been estimated to be ±30 nm.[24]

Monolayer graphene is grown by chemical vapor deposition (CVD) essentially as described.[17] Briefly, a 25-μm thick copper foil (Alfa Aesar cat #13382) is cut into 5-cm squares. The copper foil is loaded onto the center of a quartz CVD chamber, and the furnace is heated to ≈1025°C under the flow of hydrogen gas (~1,000 sccm). After 30-min annealing, the CVD growth was carried out with 20-torr total pressure with methane gas (~20 sccm) and hydrogen gas (~1,000 sccm) for 15 min. The chamber was then cooled to room temperature.

The graphene monolayer is transferred from the Cu foil onto the gold nanopyramid surface by coating the graphene-on-Cu surface with polymethyl methacrylate, dissolving the Cu in iron nitrate, and then lifting the graphene from the solution with a silicon wafer, followed by polymethyl methacrylate removal with acetone, two washes in water, and finally lifting the graphene monolayer from the surface with the nanopyramid substrate.[17,25,26] This produces the graphene–gold nanopyramid hybrid surface with <5% of the graphene surface displaying holes or cracks.[26] Platforms can be fabricated with user-determined areas. We typically use platforms of ~1 cm^2.

2.3 | Scanning electron microscopy

Scanning electron microscopic (SEM) analysis was performed using FEI Nova Nano SEM 230 instrument, an accelerating voltage of 10 kV and a beam current of 0.14 A. After the production of the gold pyramids, as described above, the substrate was mounted onto an SEM stub using double-sided adhesive tape. Imaging was performed at magnifications ranging from 30,000 to 200,000.

2.4 | Micro-Raman spectroscopy

A 20-μl volume of Aβ42 was pipetted onto the center of the platform and then immediately dried in vacuo. Raman spectra were measured using a Renishaw inVia microscope under ambient conditions. Excitation was accomplished using a GaAlAs diode laser of wavelength 785 nm. A laser power of 0.5 mW, a grating of 1,800 lines/mm, and an objective lens of 50× were used. A step size of 200 nm was used for Raman mapping. Raman data were analyzed using Renishaw WiRE 4.2 software. Strong hotpots appear in between pyramids and at their apices.[17]

2.5 | Synthesis of Aβ

Aβ was synthesized in the UCLA Biopolymer facility and then purified and characterized, as described previously.[27] Briefly, peptide synthesis was performed on an automated peptide synthesizer (model 433A, Applied Biosystems, Foster City, CA, USA) using 9-fluorenylmethoxycarbonyl-based methods on preloaded Wang resins. Aβ was purified to >97%, using reverse-phase high-performance liquid chromatography. Quantitative amino acid analysis and mass spectrometry yielded the expected composition and molecular weight. Purified peptides were stored as lyophilizates at −20°C.

2.6 | Preparation of Aβ

Aβ was prepared by dissolution in 10% (v/v) 60-mM NaOH, 45% (v/v) Milli-Q water, and 45% (v/v) 22.2-mM sodium phosphate, pH 7.4, to yield a nominal Aβ concentration of 1 mg/ml in 10-mM sodium phosphate, pH 7.4. The Aβ solution was then sonicated for 1 min in a bath sonicator (Branson Model 1510, Danbury, CT, USA) and filtered through a prewashed 30,000 molecular weight cut-off Microcon centrifugal filter device (Millipore, Billerica, MA, USA) for 15 min at 16,000 × g. The concentration of Aβ in the eluate was determined using UV absorbance (ε_{280} = 1,280 cm^{-1} M). The peptide was diluted with 10-mM sodium phosphate, pH 7.4, to a final concentration of 20 μM before use. Serial dilutions were then done in 10-mM sodium phosphate, pH 7.4. All measurements were performed at 22°C. This protocol reproducibly yields aggregate-free Aβ monomer in rapid equilibrium with low order oligomers, which is termed low molecular weight Aβ.[28]

2.7 | Histograms of signal intensity

The signal intensities observed at 935 cm^{-1} in samples analyzed at concentrations of 10^{-17}, 10^{-15}, and 10^{-13} M were incorporated into a data table (see text for rationale), each element of which represented the intensity from a single hot spot. The total numbers of hot spots at which signals were observed, n_i, were 14 (10^{-17} M), 100 (10^{-15} M), and 200 (10^{-13} M). To produce a histogram of

intensities, individual intensities were binned using a bin size of 100 μAU. Frequencies were calculated according to the formula $f_i = n_i/n_t \times 100$; in which f_i is percent frequency of occurrence of intensity i, n_i is the number of observations of intensity i, and n_t is the total number of intensity observations. The weighted average intensity for the histogram envelope observed in the 10^{-17}-M sample was calculated according to the formula $I_{avg} = \sum_{a=1*10^{-4}AU}^{\infty} i_a * n_i/n_t$. Plots were done using Origin v8.4.

3 | RESULTS AND DISCUSSION

We used SEM to examine the surface morphology of the platforms after fabrication to confirm the presence of the pyramid structures, prior to the addition of graphene. We observed that the pyramids form a quasiperiodic array of hexagonal arrangement uniformly distributed over the surface (Figure 1a). Some variations (±30 nm) are observed in the spacing between pyramids and the sizes of the pyramids (±30 nm), as expected based on the fabrication process.[24]

To examine the quantification characteristics of the graphene monolayer coated gold-nanopyramid hybrid platform, we studied the 42-amino acid form of Aβ, Aβ42, which is thought to be a seminal pathologic agent in Alzheimer's disease[31] and is used as a disease biomarker.[32] We initially applied a 20-μM solution of freshly prepared, unaggregated, low molecular weight Aβ[33] to our platforms. Aβ42 is known to aggregate into oligomers and fibrils over time,[34] so to ensure that our starting samples did not aggregate during preparation for SERS, we prepared the samples rapidly (<10 min) at low temperature (4°C) following a stringent solubilization and filtration procedure.[28] We acquired spectra immediately after preparation and periodically thereafter. Examination of these spectra showed that no observable aggregation occurred within 10 min. (Figure S1).[35] In addition, when experiments at Aβ concentrations in the submicromolar regime are performed, rates of simple collision-induced aggregation or nucleation-dependent polymerization are so low that no substantial aggregation occurs.[36] Figure 1b shows a typical SERS spectrum of Aβ42. We also acquired Raman spectra for sodium phosphate buffer alone and did not observe any Raman peaks (Figure S2). This indicated that all the peaks we observed were from graphene or Aβ42. Several characteristic Raman peaks were observed, including those due to Tyr (823 and 850 cm^{-1}), carbon–carbon (C–C) stretching (935 cm^{-1}), Phe (982 and 1,450 cm^{-1}), Lys or Asn (1,087 cm^{-1}), Val or Ile (1,124 cm^{-1}) and graphene D (1,350

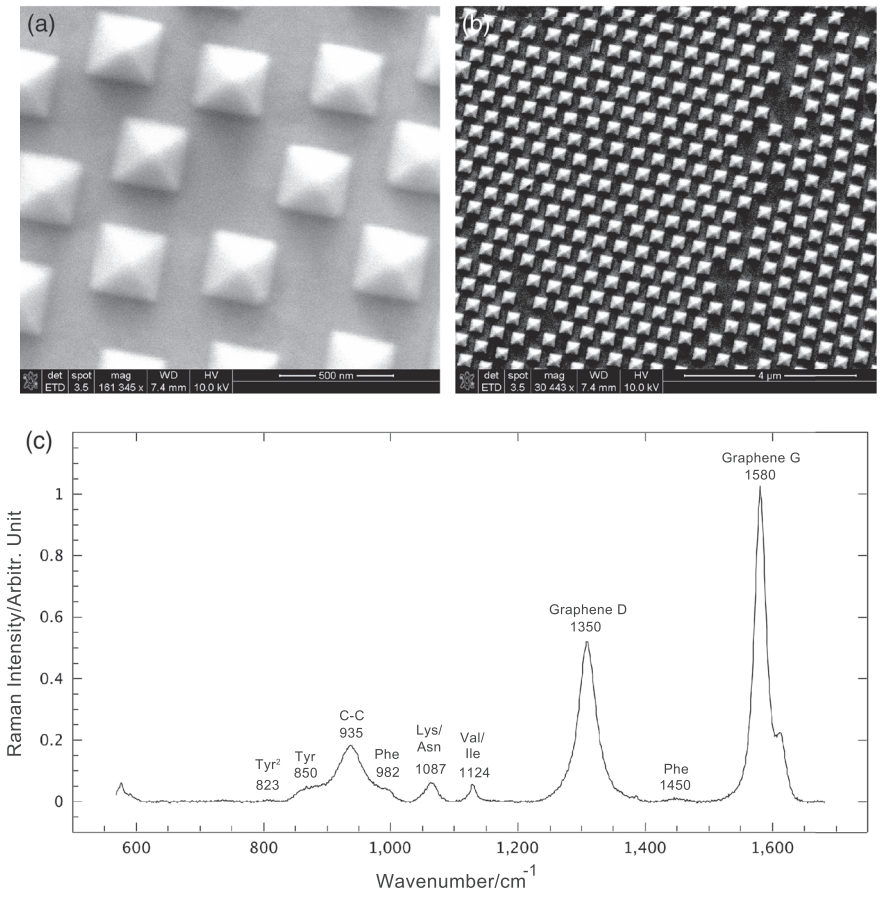

FIGURE 1 Hybrid Platform and Raman spectrum of Aβ42. (a) Scanning electron microscopy images of the gold pyramid structure at magnifications of 30,443 (right panel) and 161,345 (left panel). (b) Aβ42 was prepared at a concentration of 20 μM, pH 7.4, and applied to the platform. Abscissa indicates wavenumber (cm^{-1}). Peaks were assigned based on published results.[29,30] Wavenumber assignments are 559, aliphatic; 575, C–C bond stretching mode; 823, out-of-plane ring breathing vibration or double Tyr (Tyr2); 850, single bond stretching for Tyr and Val; 935, number of carbon -carbon bonds of protein backbone or Gly; 982, C–C stretching in β-sheets or part of Phe; 1,000, Lys or Asn; 1,124, Val or Ile; 1,350, graphene D peak;1,450, CH2 bending or Phe; 1,580, graphene G peak

cm^{-1}), G peaks (1,580 cm^{-1}), and D' peak (1,588 cm^{-1}).[29,30] We note that an amide I peak (1,650 cm^{-1}) appears near the graphene G peak, but no overlap is observed.

To establish the quantitative ability of the hybrid platform, Aβ42 at concentrations ranging from 10^{-21} to 10^{-9} M was applied to the substrate, and spectra were acquired (Figure 2a). Based on earlier reports by Wang et al. wherein they showed that the intensity of graphene G peak (peak height) correlated with hot spot intensity by mapping of the graphene–gold nanopyramid hybrid substrate surface, we reasoned that the graphene G peak intensity could be used to normalize the observed protein peak intensity.[17,37] Wang et al. showed that the intensity of the protein peak (in that case, lysozyme) was mapped over an area of varying hot spot intensity, and the intensity of the peaks correlated linearly with that of the graphene G peak.[17] The graphene G peak intensity (peak height) was correlated to both the graphene configuration and EM field intensity.[17] To implement this, the Aβ42 spectra were normalized to the graphene G peak (1,580 cm^{-1} peak height) to account for any variation in the local EM field intensity among the various hot spots. This normalization allowed us to examine if the Raman peak intensity of Aβ42 correlated with its concentration. We normalize using the peak height at 1,580 cm^{-1}, without peak fitting, as we expect these methods to give similar results[38] particularly because the nearest peak is not close enough to influence the peak maximum at 1,580 cm^{-1}. Graphene was confirmed to be exclusively a single atomic layer using the characteristics of the graphene 2D band (data not shown) prior to transfer onto the gold nanopyramid substrate.[37] Changes in the graphene G peak intensity thus should arise solely from changes in the EM field and thus can be used to normalize protein peak intensities obtained across the substrate surface. The graphene G peaks among spectra superimpose as a result of the normalization. The peaks at 1,350 cm^{-1} did not superimpose as did the G peaks, so we wondered if their intensities correlated with the intensity of the protein C–C peak at 935 cm^{-1}. We plotted the intensity of each wavenumber for concentrations from 10^{-9} to 10^{-13} to answer this question and found that there was little (R^2 = 0.23) correlation of these values (Figure S3). The 1,350-cm^{-1} peak is the graphene D peak, which results from the sp^3 atoms in the carbon ring structure.[39] The D peak is related to defects in the graphene, especially graphene folds formed when the nearly planar graphene is overlaid on the pyramids of the platform. As such, the D peak is a function of surface topology and not suitable for use as a normalization signal.[37]

We observed no qualitative differences among the spectra obtained at different Aβ42 concentrations. Instead, as expected, a direct relationship between peak intensity and concentration was seen. At a single hot spot, at which multiple analytes can bind, Raman signal intensity is the sum of the individual intensities of all the Raman active analytes present. Increases in signal intensity with analyte concentration are thus observed until the limited volume of the hot spot is fully occupied by

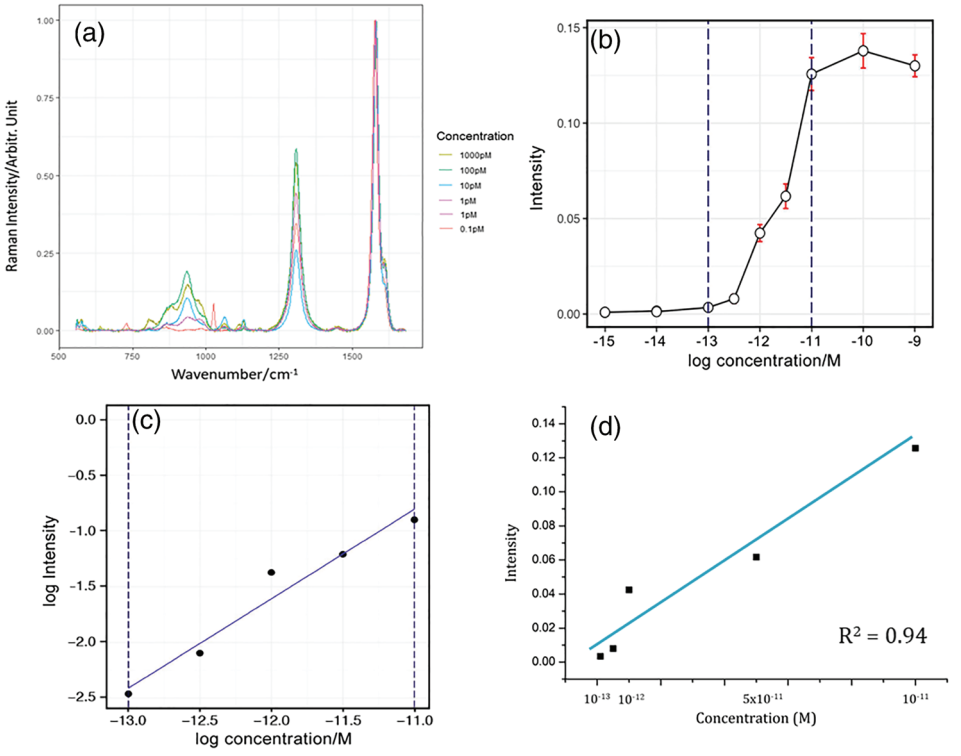

FIGURE 2 Concentration-dependence of Raman signal intensities. (a) Spectra of Aβ42 at concentrations ranging from 10^{-13} to 10^{-9} M. Spectra from concentrations of 10^{-15} and 10^{-14} were obtained but they are not shown because they are essentially flat in this representation. (b) Normalized peak intensity (AU) of the 935 cm^{-1} peak. All points are the averages of three replicates. Red bars signify standard deviations. If error bars are not visible, this indicates that the size of the standard deviation was less than the size of the data point. (c) Log–log plot of the data from panel B. The blue line was produced by linear regression analysis (R^2 = 0.97). (d) Linear regression plot of the data from panel B with R^2 = 0.94

analyte molecules, after which increases in analyte concentration do not lead to increased peak intensity (Figure 3). This is seen clearly in Figure 2b, in which the concentration dependence of peak intensity at 935 cm^{-1} is shown. The data produce a sigmoidal curve within which a quasilinear region is seen extending from ~10^{-13} to 10^{-11} M (Figure 2b; between dashed lines). The linearity within this region is more apparent from examination of a log–log plot (Figure 2c), which we utilize because of the very broad concentration regime studied. Regression analysis of this region produces a line with a correlation coefficient of 0.94 (Figure 2d). From the peaks emanating from protein, the 935 cm−^{1} peak has the highest relative peak intensity and the lowest signal/noise ratio. As such, experimental noise has less impact on its intensity, and thus, the linear relationship between intensity of the 935 cm^{-1} peak and concentration provides a more accurate quantitation than the use of more isolated vibrational modes at 1,087 and 1,124 cm^{-1} (Figure S4). We observed increasing protein concentration towards the perimeter of the applied droplet, induced by the surface tension of the liquid during drop casting, likely due to the "coffee ring" effect. We find that the concentration change is not high enough to influence the linear relationship between protein concentration and peak intensity (c.f. error bars on Figure 2b). One explanation for the linearity of increasing SERS intensity with increasing concentration is that many protein molecules can fit within a single hot spot before it is filled, which would be difficult to observe if the hot spot size is closer to the size of a single analyte molecule.

As analyte concentration decreases, not all hot spots will have adsorbed analytes, and a direct relationship between peak intensities and analyte concentration does not exist (Figure 4). For this reason, instead of quantifying signal intensities at individual hot spots, we implement a quantification method that considers instead the frequency of hot spots from which Raman spectra signals of the analytes are detectable. To determine this frequency, we scanned relatively large areas (~50 × 50 μm) of the hybrid platform using Raman mapping at a step size of 1 μm (i.e., a 1-μm^2 area of pixels for each

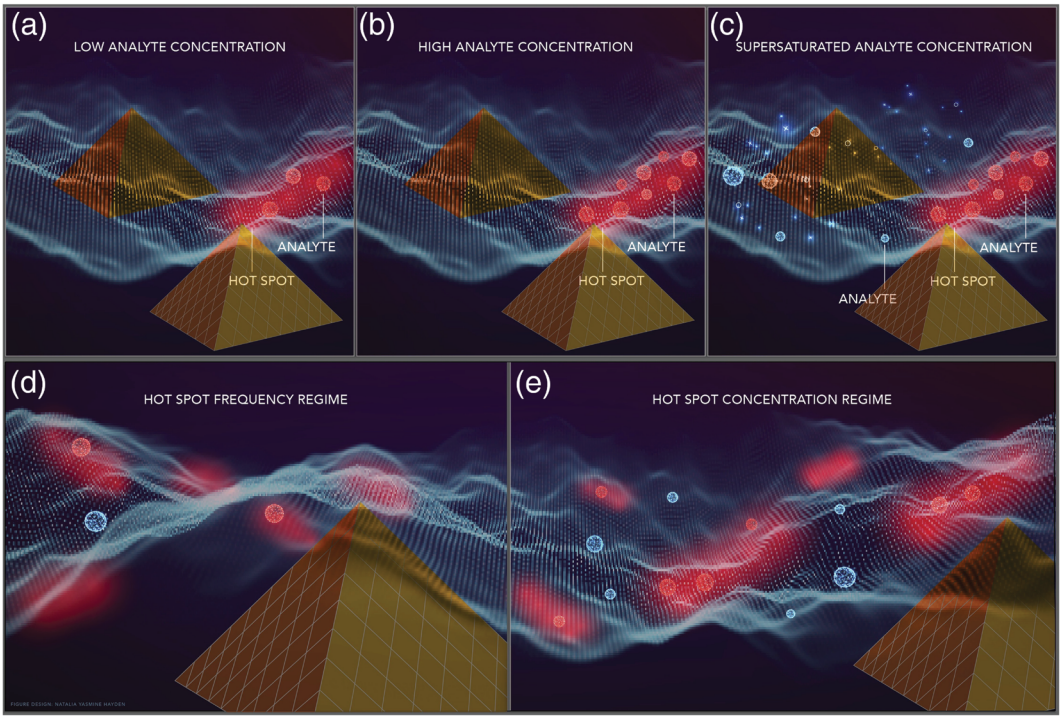

FIGURE 3 (a–c) Dependence of Raman signal intensity on analyte number concentration at hot spots. In analyte concentration regimes in which essentially all hot spots (red clouds) contain at least one analyte molecule, Raman signal intensity depends on analyte number concentration (a). Signal intensity thus increases with analyte concentration (b) until hot spots are saturated with analytes (c), at which time accurate determination of concentration is no longer possible because not all analytes are associated with hot spots. (d–e) Hot spot occupancy versus analyte concentration. As illustrated in (d), at lower concentrations, hot spot occupancy is <100%, and peak intensities begin to correlate with the probability of an individual protein molecule being collocated with a hot spot, as opposed to the number of molecules at each hot spot (as in the high concentration regime). In the low concentration regime, quantification is accomplished by determination of occupancy frequency per se. Panel (e) illustrates a concentration regime in which most or all hot spots contain at least one analyte molecule. Hot spot occupancy thus is ≅100%, and signal intensity depends on the number of analyte molecules. Analyte molecules within a hot spot are shown in red. Analytes outside of hot spots are blue

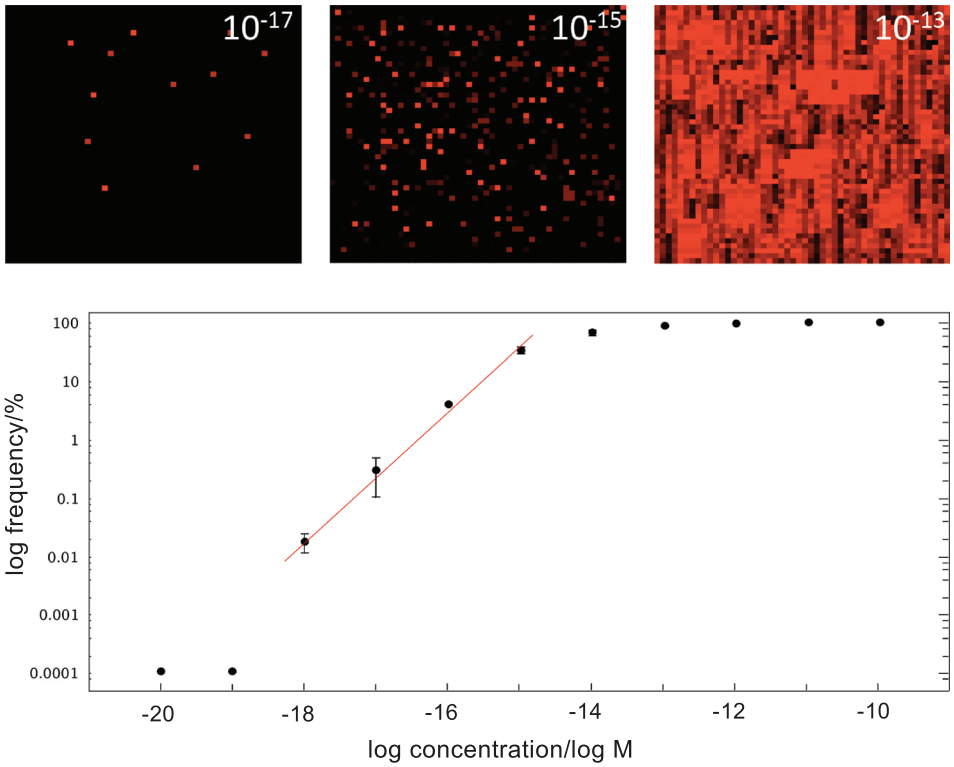

FIGURE 4 Determination of peptide concentration using hot spot signal frequency measurements. Upper panel: Intensity mapping of the 935 cm^{-1} peak at concentrations of 10^{-13}, 10^{-15}, and 10^{-17} M. The step size of the mappings was 1 μm, and 2,600 spectra were acquired at each concentration. Lower panel: A log–log plot of concentration (M) versus hot spot signal frequency (%) determined in the concentration range of 10^{-20} to 10^{-10} M. For ease of visualization, points at 10^{-20} and 10^{-19} M, which had zero intensity, are plotted with frequencies of 0.0001%. Solid line shows result of linear regression analysis in the concentration regime 10^{-18} to 10^{-15} M, inclusive (correlation coefficient $R^2 = 0.97$). Data were obtained from two independent experiments and are shown as averages plus the frequency ranges (shown as black bars) produced by the two points. Where the black bars are not visible, this indicates that the range was smaller than the diameter of the point indicating the average frequency [Colour figure can be viewed at wileyonlinelibrary.com]

measurement). This scanning encompasses the entire area of the original droplet, including the outer perimeter and inside of the dried ring, so that we get a representative sampling of the protein concentration. We performed this scanning on platforms on which we applied Aβ42 in concentrations ranging from 10^{-18} to 10^{-10} M. Figure 5 (upper panels) shows heat maps of the intensity data collected at concentrations of 10^{-13}, 10^{-15}, and 10^{-17} M. Inspection reveals a substantial concentration-dependent decrease in frequency. A plot of the frequency distribution (Figure 5, lower panel) shows that no signals were observed at Aβ42 concentrations of 10^{-20} or 10^{-19} M. A direct relationship between frequency and concentration was observed between 10^{-18} to 10^{-15} M (Figure 5, lower panel, solid line). Above 10^{-15} M, a concentration regime is encountered in which the majority of hot spots have at least one Aβ peptide, and increasing Aβ concentration results in an increase in the number of peptides per pyramid but not in a substantial increase in the percentage of pyramids with at least one peptide (Table 1). Table 1 shows the frequency of observable spectra in each of the reported concentrations, from two independent experiments, which is the number of detectable signals divided by the total number of scans across the area examined. If analyte concentration is within the transition region between partial and full hot spot occupancy, simple dilution will allow accurate quantification based solely on occupancy frequency. We note that Pérez-Ruiz et al., in studies determining tau concentrations,[40] have also successfully employed a frequency approach (cf. Figure 5 of this manuscript with fig. 5 of Pérez-Ruiz et al.). This approach enabled attomolar limits of detection depending on whether samples were prepared in buffer (24 aM) or blood plasma (55 aM). Coupled with analogue measurements at higher concentrations, a dynamic concentration range of six orders of magnitude could be obtained. These capabilities compare favorably with our own—a dynamic range of seven orders of magnitude and a limit of detection of 1 aM.

It should be pointed out that the true detection limit is when the concentration of the analyte becomes so low that the probability of a single molecule existing within a

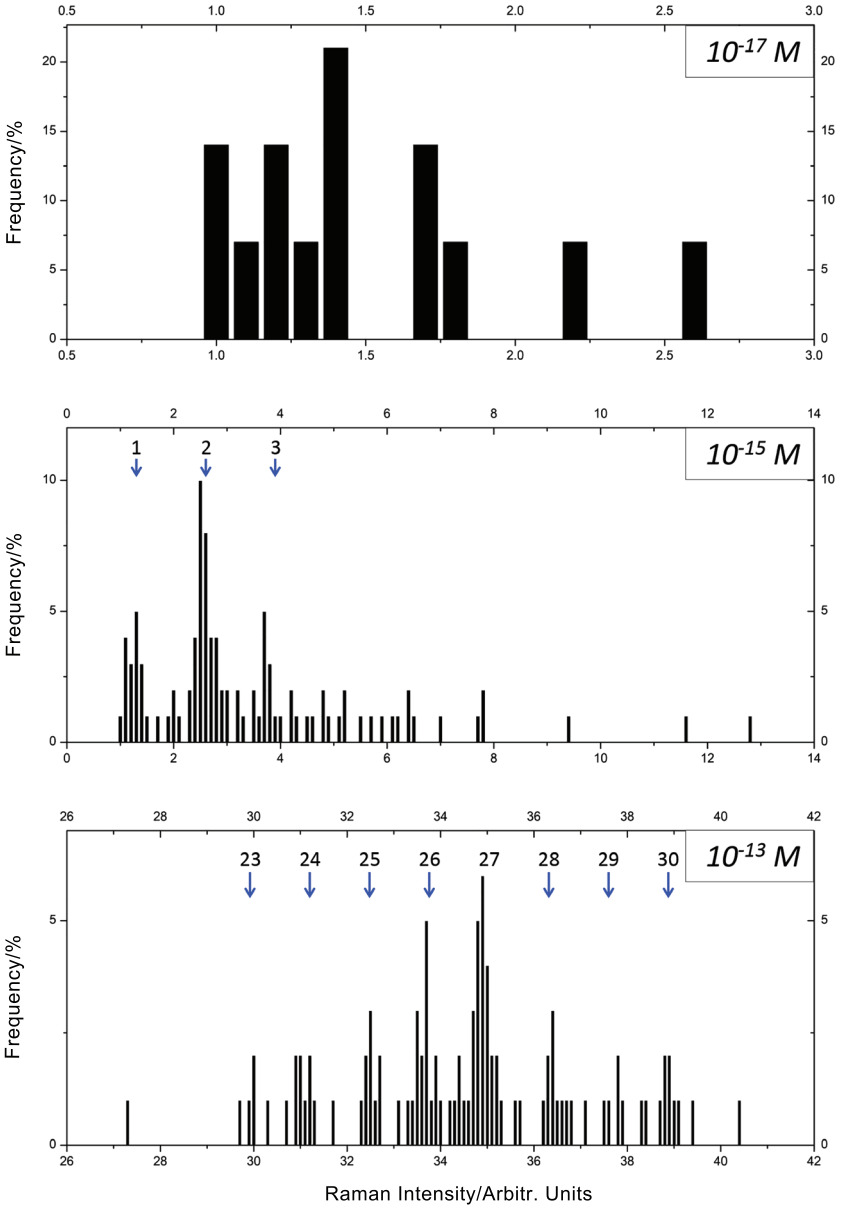

FIGURE 5 Hot spot intensities. The graphene normalized signal intensities of the 935 cm^{-1} Raman peak acquired at Aβ concentrations of 10^{-17}, 10^{-15}, and 10^{-13} M are presented in histograms. Axes are frequency (ordinate) and normalized intensity (abscissa). Numbers at blue arrows signify the number of monomers producing the observed intensities [Colour figure can be viewed at wileyonlinelibrary.com]

TABLE 1 Hot spot signal frequency versus Aβ42 concentration

Concentration (log M)	−20	−19	−18	−17	−16	−15	−14	−13	−12	−11	−10
Frequency (Exp. #1) (%)	0.000	0.000	0.023	0.470	4.12	38.4	72.2	84.9	95.2	100	100
Frequency (Exp. #2) (%)	0.000	0.000	0.011	0.102	3.85	28.7	59.2	87.2	96.0	100	100

Note. The frequencies of observable signals from hot spots were determined over a concentration range of 10^{-18} to 10^{-10} M in two independent experiments. Frequency (%) = 100 × (number of hot spots with detectable signal)/(total number of hot spots).

20-μL droplet is <1. This probability is 0.37 at 10^{-19} M. This explains why, in practice, no Aβ signal was observed at lower concentrations. In theory, there is a finite probability that a single molecule will exist within an applied volume at any concentration and that a spectroscopist can spend sufficient time to find its location and signal on the platform.

We next sought to determine, in the frequency regime of concentration, how intensity was related to number of analyte molecules per hot spot. To do so, we created histograms of normalized spectral intensities at the same concentrations in Figure 5 (10^{-17}, 10^{-15}, and 10^{-13} M). We used the intensity of the 935 cm^{-1} peak (C–C bonds) for this purpose, as this peak had been used to quantify Aβ concentration (Figure 2). Our expectation was that the lowest observed intensity should be produced by a single analyte molecule and that subsequent signal intensities should be integer multiples of that lowest intensity.

In Figure 5, we observed a single node with an average intensity of $1.3 \times 10{-}^{4}$ AU. At a concentration of 10^{-15} M, this node was also observed, in addition to prominent nodes at intensities that were double or triple that intensity. This shifting of the overall frequency distribution to higher intensities was seen at 10^{-13} M as well, a concentration that produced nodes (blue arrows) at intensities that were 23- to 30-fold larger than the lowest intensity node, consistent with the conclusion that this distribution reflected hot spots containing 23–30 analyte molecules. When we compared the average signal intensities for each node envelope with those predicted based on multiples of 1.3×10^{-4} AU per monomer, we observed remarkable agreement (mean and standard deviation of the differences was $0.04 \pm 0.09 \times 10^{-4}$ AU; Table 2). These data support the conclusion that we are, at minimum, able to differentiate signals produced by 1–30 peptides per hot spot.

TABLE 2 Agreement of predicted and observed weighted average hot spot intensities

Peptides per hot spot	Predicted intensity[a]	Observed intensity[a]
1	1.3	1.3
2	2.6	2.5
3	3.9	3.7
4	5.2	–
5	6.5	6.3
6	7.8	7.7
7	9.1	9.0
8	10.4	10.5
9	11.7	11.7
10	13.0	12.8
11	14.3	14.2
12	15.6	15.6
13	16.9	16.8
14	18.2	–
15	19.5	–
16	20.8	–
17	22.1	–
18	23.4	–
19	24.7	–
20	26.0	–
21	27.3	–
22	28.6	–
23	29.9	30.0
24	31.2	31.1
25	32.5	32.5
26	33.8	33.7
27	35.1	34.9
28	36.4	36.4
29	37.7	37.8
30	39.0	38.9

Note. Leftmost column displays number of Aβ monomers per hot spot. "Predicted intensity" is number of peptides times intensity per peptide (1.3). "Observed intensity" is experimentally observed intensity. Hyphens denote intensities not observed experimentally.

[a]Units are AU × 10.[4] Data from all concentrations between 10^{-17} to 10^{-13}, inclusive, were included in the table.

Raman intensities of proteins depend not only on analyte quantity per hot spot, but on the structure of the protein, its orientation relative to the hot spot surface, and the EM field intensity. Our normalization procedure controls for the latter factor. The variation in the former two factors is reflected in the widths of the overall intensity envelopes observed in the histograms. These increase with concentration, but even at a concentration of 10^{-13} M, we see that the envelopes reflect a discrete range of analyte numbers, as opposed to including intensities from the continuum of possible analyte numbers per hot spot. This likely reflects the fact that the application and binding of protein to the matrix of pyramids is consistent with simple laws of mass action.

4 | CONCLUSION

This work demonstrates the quantification ability of the graphene–gold hybrid SERS platform using Raman mapping. The platform exhibits a linear relation between peak intensity and concentration at single hot spots (high analyte concentration), as well as a linear relationship between detection frequency and analyte concentration when scanning multiple hot spots (low analyte concentration). The platform is capable of single-molecule detection. The useful dynamic range of the hybrid platform of seven orders of magnitude (three orders of magnitude for higher concentration and four orders of magnitude of lower concentration) offers the possibility that the platform could be useful in a broad range of applications such as early stage diagnosis of Alzheimer's disease.

ACKNOWLEDGEMENTS

We acknowledge the support of the Alexander von Humboldt-Siftung Foundation (Y.-H.X.) and the National Institutes of Health (NS038328 and AG041295; D.B.T.). We are extremely grateful to Natalia Yasmine Hayden, BFA, for expert creative direction and the design of Figure 3. This work was funded in part (XY, OL, and YHX) by the Zhejiang University Cao Guangbiao High-Tech Talent Fund and a grant from the United States Government and the generous support of the American people

through the United States Department of State and the United States Agency for International Development (USAID) under the Pakistan–U.S. Science & Technology Cooperation Program. The contents do not necessarily reflect the views of the United States Government.

ORCID

Xinke Yu https://orcid.org/0000-0002-3485-9468
Eric Y. Hayden https://orcid.org/0000-0001-6977-5056
Ming Xia https://orcid.org/0000-0001-6028-4437
David B. Teplow https://orcid.org/0000-0002-2389-3417

REFERENCES

[1] V. C. Coffman, J.-Q. Wu, *Trends Biochem. Sci.* **2012**, *37*, 499.
[2] Y. Hayashi, R. Matsuda, T. Maitani, K. Imai, W. Nishimura, K. Ito, *Maeda M Anal Chem* **2004**, *76*, 1295.
[3] M. Navratil, G. A. Mabbott, E. A. Arriaga, *Anal. Chem.* **2006**, *78*, 4005.
[4] J. J. Pitt, *Clin. Biochem. Rev.* **2009**, *30*, 19.
[5] T. Lemma, A. Saliniemi, V. Hynninen, V. P. Hytönen, J. J. Toppari, *Vib Spectrosc* **2016**, *83*, 36.
[6] K. E. Stephen, D. Homrighausen, G. DePalma, C. H. Nakatsu, J. Irudayaraj, *Analyst* **2012**, *137*, 4280.
[7] A. Lorén, J. Engelbrektsson, C. Eliasson, M. Josefson, J. Abrahamsson, M. Johansson, K. Abrahamsson, *Anal. Chem.* **2004**, *76*, 7391.
[8] K. A. Antonio, Z. D. Schultz, *Anal. Chem.* **2013**, *86*, 30.
[9] S. D. Hudson, G. Chumanov, *Anal. Bioanal. Chem.* **2009**, *394*, 679.
[10] K. Kneipp, H. Kneipp, J. Kneipp, *Acc. Chem. Res.* **2006**, *39*, 443.
[11] W. Xie, S. Schlücker, *Phys. Chem. Chem. Phys.* **2013**, *15*, 5329.
[12] X. Liu, Y. Shao, Y. Tang, K.-F. Yao, *Sci. Rep.* **2014**, *4*, 1.
[13] Z.-S. Wu, G.-Z. Zhou, J.-H. Jiang, G.-L. Shen, R.-Q. Yu, *Talanta* **2006**, *70*, 533.
[14] N. B. Colthup, L. H. Daly, S. E. Wiberley, *Introduction to infrared and Raman spectroscopy*, 3rd ed., Academic Press, Boston **1990**.
[15] W. Xu, X. Ling, J. Xiao, M. S. Dresselhaus, J. Kong, H. Xu, Z. Liu, J. Zhang, *Proc. Natl. Acad. Sci. U. S. A.* **2012**, *109*, 9281.
[16] D. Zhang, Y. Xie, S. K. Deb, V. J. Davison, D. Ben-Amotz, *Anal. Chem.* **2005**, *77*, 3563.
[17] P. Wang, O. Liang, W. Zhang, T. Schroeder, Y. H. Xie, *Adv. Mater.* **2013**, *25*, 4918.
[18] X. Ling, L. M. Xie, Y. Fang, H. Xu, H. L. Zhang, J. Kong, M. S. Dresselhaus, J. Zhang, Z. F. Liu, *Nano Lett.* **2010**, *10*, 553.
[19] X. Ling, L. G. Moura, M. A. Pimenta, J. Zhang, *J. Phys. Chem. C* **2012**, *116*, 25112.
[20] A. Rochefort, J. D. Wuest, *Langmuir* **2009**, *25*, 210.
[21] H. T. Beier, C. B. Cowan, I.-H. Chou, J. Pallikal, J. E. Henry, M. E. Benford, J. B. Jackson, T. A. Good, G. L. Coté, *Plasmonics* **2007**, *2*, 55.
[22] D. Bhowmik, K. R. Mote, C. M. MacLaughlin, N. Biswas, B. Chandra, J. K. Basu, G. C. Walker, P. K. Madhu, S. Maiti, *ACS Nano* **2015**, *9*, 9070.
[23] I. H. Chou, M. Benford, H. T. Beier, G. L. Cote, M. Wang, N. Jing, J. Kameoka, T. A. Good, *Nano Lett.* **2008**, *8*, 1729.
[24] P. Wang, M. Xia, O. Liang, K. Sun, A. F. Cipriano, T. Schroeder, H. Liu, Y.-H. Xie, *Anal. Chem.* **2015**, *87*, 10255.
[25] X. Li, Y. Zhu, W. Cai, M. Borysiak, B. Han, D. Chen, R. D. Piner, L. Colombo, R. S. Ruoff, *Nano Lett.* **2009**, *9*, 4359.
[26] X. Li, W. Cai, J. An, S. Kim, J. Nah, D. Yang, R. Piner, A. Velamakanni, I. Jung, E. Tutuc, S. K. Banerjee, L. Colombo, R. S. Ruoff, *Science* **2009**, *324*, 1312.
[27] D. M. Walsh, A. Lomakin, G. B. Benedek, M. M. Condron, D. B. Teplow, *J. Biol. Chem.* **1997**, *272*, 22364-22372.
[28] D. B. Teplow, *Methods Enzymol.* **2006**, *413*, 20.
[29] Z. Movasaghi, S. Rehman, I. U. Rehman, *Applied Spectroscopy Reviews* **2007**, *42*, 493.
[30] A. T. Tu, A. Tu, *Raman spectroscopy in biology: principles and applications*, John Wiley & Sons, New York **1982**.
[31] S. G. Younkin, *Ann. Neurol.* **1995**, *37*, 287.
[32] N. Andreasen, L. Minthon, P. Davidsson, E. Vanmechelen, H. Vanderstichele, B. Winblad, K. Blennow, *Arch. Neurol.* **2001**, *58*, 373.
[33] E. Y. Hayden, G. Yamin, S. Beroukhim, B. Chen, M. Kibalchenko, L. Jiang, L. Ho, J. Wang, G. M. Pasinetti, D. B. Teplow, *J. Neurochem.* **2015**, *135*, 416.
[34] R. Roychaudhuri, M. Yang, M. M. Hoshi, D. B. Teplow, *J. Biol. Chem.* **2009**, *284*, 4749.
[35] X. Yu, E. Y. Hayden, M. Xia, O. Liang, L. Cheah, D. B. Teplow, Y. H. Xie, *Protein Sci.* **2018**, *27*, 1427.
[36] E. Hellstrand, B. Boland, D. M. Walsh, S. Linse, *ACS Chem. Nerosci.* **2010**, *1*, 13.
[37] P. Wang, W. Zhang, O. Liang, M. Pantoja, J. Katzer, T. Schroeder, Y. H. Xie, *ACS Nano* **2012**, *6*, 6244.
[38] A. L. Shen, Y. C. Weng, T. C. Chou, *Zeitschrift Fur Naturforschung Section B-a Journal of Chemical Sciences* **2010**, *65*, 67.
[39] A. Ferrari, J. Meyer, V. Scardaci, C. Casiraghi, M. Lazzeri, F. Mauri, S. Piscanec, D. Jiang, K. Novoselov, S. Roth, *Phys. Rev. Lett.* **2006**, *97*, 187401.
[40] E. Pérez-Ruiz, D. Decrop, K. Ven, L. Tripodi, K. Leirs, J. Rosseels, M. van de Wouwer, N. Geukens, A. De Vos, E. Vanmechelen, J. Winderickx, J. Lammertyn, D. Spasic, *Anal. Chim. Acta* **2018**, *1015*, 74.

SUPPORTING INFORMATION

Additional supporting information may be found online in the Supporting Information section at the end of this article.

How to cite this article: Yu X, Hayden EY, Wang P, et al. Ultrasensitive amyloid β-protein quantification with high dynamic range using a hybrid graphene–gold surface-enhanced Raman spectroscopy platform. *J Raman Spectrosc*. 2020;51: 432–441. https://doi.org/10.1002/jrs.5785